# Opto-fluidic micro-ring resonator for sensitive label-free viral detection

**Hongying Zhu,[a] Ian M. White,[a] Jonathan D. Suter,[a] Mohammed Zourob[b] and Xudong Fan*[a]**

***Received 31st October 2007, Accepted 8th December 2007***
***First published as an Advance Article on the web 8th January 2008***
**DOI: 10.1039/b716834a**

We have demonstrated sensitive label-free virus detection using the opto-fluidic ring resonator (OFRR) sensor. The OFRR is a novel sensing platform that integrates the microfluidics and photonic sensing technology with a low detection limit and small volume. In our experiment, filamentous bacteriophage M13 was used as a safe model system. Virus samples were flowed through the OFRR whose surface was coated with M13-specific antibodies. We studied the sensor performance by monitoring in real-time the virus and antibody interaction. It is shown that OFRR can detect M13 with high specificity and sensitivity. The detection limit is approximately $2.3 \times 10^3$ pfu mL$^{-1}$ and the detection dynamic range spanned seven orders of magnitude. Theoretical analysis was also carried out to confirm the experimental results. Our study will lead to development of novel OFRR-based, sensitive, rapid, and low-cost micro total analysis devices for virus detection.

## Introduction

Detection and identification of viruses are critically important in many fields such as healthcare and counter-bioterrorism. To prevent and control the spread of viruses, there is an urgent need for an analysis device that can rapidly detect viruses with high specificity and sensitivity. Polymerase chain reaction (PCR)[1–4] and enzyme-linked immunosorbent assay (ELISA)[5,6] are traditional methods for routine virus detection in medical laboratories. Both techniques are very sensitive; for example, real-time PCR can achieve the detection of one virus per reaction.[7] However, these techniques have some intrinsic limitations like relatively low versatility, difficulty with multiplexing the assay, and high equipment cost. Moreover, they involve labor-intensive and time-consuming laboratory procedures and trained personnel are needed. This motivates much interest in developing easy techniques for quick virus detection.

In recent years, non-destructive biosensor techniques have been becoming more prevalent and have shown great potential for viral detection, especially label-free detection methods, such as the quartz crystal microbalance (QCM),[8–11] the surface acoustic wave (SAW) resonator,[12] surface plasmon resonance (SPR),[13–15] fiber optics,[16] and interferometers,[17] *etc.*, with detection limits ranging from $10^5$ pfu mL$^{-1}$ to $10^9$ pfu mL$^{-1}$. More recently, the Young interferometer and microsphere ring resonator have been employed for sensitive virus detection.[18,19] However, these methods either need an external fluidics channel to transport the sample to the detection zone, or require a sophisticated detection system, which increase the experimental cost and time. Herein, we have developed a novel opto-fluidic ring resonator (OFRR) sensor for label-free virus detection with distinguished advantages over existing techniques.

The OFRR is a novel sensing platform developed recently and has been used for applications such as biomolecule detection, capillary electrophoresis, and dye laser development.[20–24] The principle of the OFRR is shown schematically in Fig. 1(A). It employs a thin-walled micro-sized capillary. The capillary serves as the microfluidics for sample transport and the circular cross section of the capillary forms a ring resonator to support the circulating mode called whispering gallery modes (WGMs), which can be launched by placing the OFRR in touch with the fiber taper perpendicular to the OFRR. When the laser wavelength meets the resonant condition, the light is trapped into the OFRR, causing a reduction in the power measured at the fiber output, which can be used to indicate the WGM spectral position. The capillary wall is sufficiently thin (<4 μm) so that the evanescent field of the WGM can extend into the capillary core, where it repeatedly interacts with the analyte.

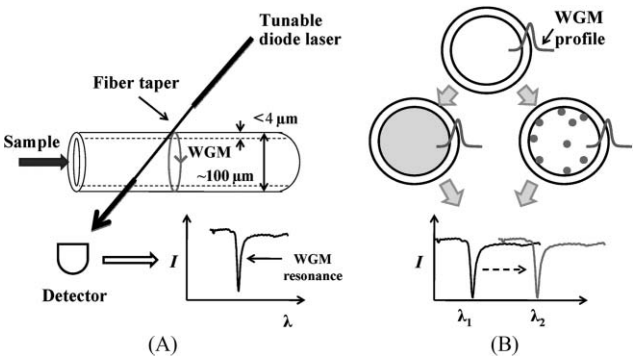


**Fig. 1** (A) Overall configuration for the OFRR. (B) The cross section of an OFRR. The WGM circulates along the OFRR circumference. Its evanescent field extends beyond the interior surface of the OFRR and interacts with the analytes in the core. The WGM resonant wavelength shifts in response to the bulk solution change or the binding of molecules to the OFRR interior surface.

[a]*Department of Biological Engineering, University of Missouri-Columbia, 240D, Bond Life Sciences Center, Columbia, MO 65211, USA. E-mail: fanxud@missouri.edu; Fax: +573-884-9676; Tel: +573-884-2543*
[b]*Biosensors Division, Biophage Pharma, 6100 Royalmount Montreal, QC, Canada H4P 2R2*

 

As shown in Fig. 1(B) the OFRR performs label-free sensing by detecting the refractive index (RI) changes in the core. It can be induced by the change of bulk solution in the core or the binding of the biomolecules to the sensor surface. The relation between the WGM shift and the RI is shown as follows,

$$2\pi R n_{\text{eff}} = m\lambda \quad (1)$$

where $n_{\text{eff}}$ is the effective RI of the media experienced by the WGMs, $R$ is the capillary radius, $m$ is an integer representing the WGM angular momentum, and $\lambda$ is the WGM resonant wavelength. When target biomolecules are captured to the OFRR interior surface, the RI near the OFRR surface changes, resulting in a WGM resonant wavelength shift. Therefore, the resulting transduction signal reveals the quantitative and kinetic information for biomolecule interactions on the OFRR surface. The OFRR has been successfully applied to the detection of protein and DNA, with an RI detection limit of $10^{-7}$ refractive index units (RIU) and a mass detection limit of sub-pg mm$^{-2}$,[21,22] competitive with commercialized SPR-based label-free biosensors.

The OFRR's unique architecture makes it a very promising sensing platform for virus detection. First, the OFRR naturally integrates the ring resonator with the microfluidics channel, allowing for continuous monitoring of the liquid sample flowing in the capillary in real time. Second, the capillary channel is only a hundred micrometers in diameter, leading to very small fluid samples required for virus detection. Third, the circular nature of the capillary enables the efficient capture and rapid detection of the analyte. Fourth, the detection principle is simple and the desired OFRR can be mass-produced using a commercial fiber draw tower in a very cost-effective manner. Fifth, the OFRR can potentially be scaled up to a two-dimensional array with dimensions less than several centimeters, which is suitable for portable point-of-care devices for simultaneous on-site detection of different types of viruses.

In this paper, we will describe the use of the OFRR for rapid virus detection. M13 filamentous bacteriophage was chosen as a safe model system. M13 is about 900 nm long and 10 nm wide. It is composed of circular single-stranded DNA, encapsulated in approximately 2700 copies of the major coat protein g8p. M13 has similar molecular weight to serious human pathogens, yielding valuable information for other types of viral detection.[8] The results show that OFRR has a high sensitivity and specificity for virus detection, with a low detection limit and a wide dynamic range.

## Experimental

### Materials

98% Ethanol, 12 M HCl, 48% hydrofluoric acid (HF), 3-aminopropyltrimethoxysilane (3-APS) and 75% glutaraldehyde in water were all purchased from Sigma-Aldrich (St. Louis, MO). All chemical agents were used without purification and were prepared in 18 MΩ water generated by the Easypure-UV system from Barnstead (Dubuque, IA). The wild type M13 bacteriophage was produced and provided by Biological Science Department, University of Missouri-Columbia. T4 bacteriophage was provided by Biophage Pharma Inc. (Montreal, Canada). Anti-M13 antibody was obtained from GE Healthcare Life Sciences Division. Silica glass tubes of 1.2 mm outer diameter (OD) and 0.85 mm inner diameter (ID) were purchased from Sutter Instruments (Novato, CA).

### Experimental setup

The OFRR with 150 μm OD was fabricated by rapidly pulling a quartz capillary under heat (*ca.* 2000 °C) provided by $CO_2$ lasers. To further reduce the wall thickness to a few micrometers, diluted HF (*ca.* 10%) was pumped through the capillary by a peristaltic pump. These procedures have been described in detail in the previous work.[20] The schematic of the experimental setup is shown in Fig. 2. An optical fiber taper with a diameter of approximately 3 μm, fabricated by stretching an SMF-28 optical fiber under flame, was brought into contact with the OFRR to couple the light from a 980 nm tunable diode laser from New Focus (San Jose, CA; linewidth <3 fm) into the WGM. The laser periodically scanned the output wavelength at a rate of 5 Hz. A photodetector was used to monitor the light at the output end of the optical fiber. When the laser wavelength meets the resonant condition described in eqn (1), the light is coupled into the OFRR, causing a reduction in power measured at the fiber output, which can be used to indicate the WGM spectral position. The measurement system was controlled by a computer through a data acquisition card from National Instruments (Austin, TX) and the WGM spectral position was recorded for post-analysis.

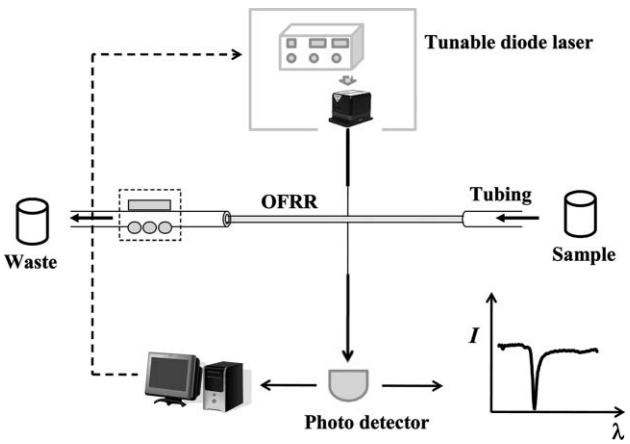


**Fig. 2** Experimental setup for virus detection.

### OFRR bulk refractive index sensitivity (BRIS) characterization

As described in the Introduction, the OFRR performs label-free sensing by measuring the WGM spectral response to the RI change in the core or near the sensing surface. The WGM spectral response to the RI change in the core is called the bulk refractive index sensitivity (BRIS). In the previous work, we developed a linear relationship between OFRR's BRIS and its response to biomolecule deposition on the sensing surface.[21] Therefore, before performing the virus detection with the OFRR, it is essential to first characterize the BRIS, which is in units of nm RIU$^{-1}$. The characterization of OFRR's BRIS was described in detail in previous work.[20] Briefly, incremental

concentrations of ethanol with known RI were pumped into the OFRR consecutively with a rinsing step between each new concentration to ensure that the surface is cleaned before the next measurement. The gradual increase in the bulk fluid RI caused the WGM to shift to a longer wavelength. The BRIS of 22 nm $RIU^{-1}$ was obtained by measuring the slope of the WGM spectral shifting *versus* the RI change, as shown in Fig. 3.

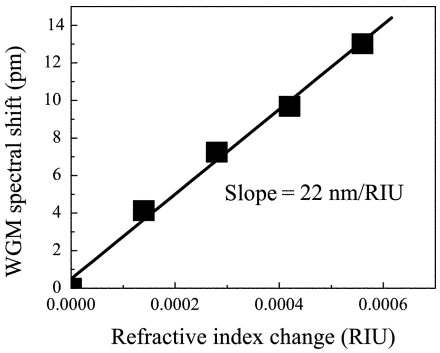


**Fig. 3** OFRR sensitivity curve with a BRIS of 22 nm $RIU^{-1}$.

### Functionalization of the OFRR interior surface

Specificity is an important feature of the biosensor. In this study antibodies were immobilized on the OFRR interior surface as the recognition element to bind the M13 bacteriophage specifically. First, the interior surface of the OFRR was cleaned with a HCl–methanol (v : v = 50 : 50) mixture and thoroughly rinsed with DI water. Then 1% 3-APS in water was passed through the OFRR for 20 min to silanize the surface. After rinsing with water, 5% homobifunctional cross-linker glutaraldehyde in water was introduced into the OFRR to link protein A to the aminated surface. Then, 0.2 mg $mL^{-1}$ protein A dissolved in 10 mM PBS buffer was run through the OFRR for 10 min. The protein A provided the binding sites for the antibody and improved the orientation of the antibody, which would increase the antibody capture capability and block the functionalized surface to reduce the non-specific adsorption. The unbound protein A was rinsed off by PBS buffer and the flow was changed to 0.1 mg $mL^{-1}$ anti-M13 monoclonal antibody in PBS buffer.

### M13 bacteriophage measurement

After surface functionalization, the OFRR was thoroughly rinsed by PBS buffer and ready for the M13 virus measurement. M13 phage was prepared in PBS buffer at different concentrations. In each measurement, M13 solution was passed through the OFRR, followed by a PBS buffer rinse to remove the unbound virus from the surface. Anti-M13 antibody is specific to the M13 coating protein. Therefore, each M13 phage has multiple binding sites for antibodies. To further confirm the measurement signal, secondary anti-M13 antibody was introduced into the OFRR. After each measurement cycle, the interior surface of the OFRR was cleaned first with a HCl–methanol mixture (v : v = 50 : 50) and then by diluted HF (*ca.* 0.5%) to completely remove all of the functional and biomolecule layers from the surface. After this, the OFRR can be used for the next measurement. The WGM spectral position was monitored and recorded by computer during the whole process of the functionalization and virus measurement for post-analysis.

## Results and discussion

### Detection of M13 bacteriophages with OFRR

First, the OFRR was employed for direct and real-time detection of M13 virus. Fig. 4 shows the time-dependent WGM spectral position shift caused by the consecutive immobilization of the biomolecular layers on the surface. The interior surface of the OFRR was modified with functional groups, as described in the Experimental section, and it was immersed in 10 mM PBS buffer (pH = 7.4) to establish the detection baseline. Then protein A in PBS was flowed through the OFRR. The protein A bound to the aminated surface caused the effective RI on the surface increase which resulted in the WGM spectral position shifting to the longer wavelength. After 20 min, the WGM shift reached the saturation level. From Fig. 4, the WGM spectral position has about a 15 pm red shift. Then 0.1 mg $mL^{-1}$ anti-M13 antibody was introduced into the OFRR and trapped by protein A, resulting in the WGM spectral red shift of 20 pm. M13 bacteriophage was introduced into the OFRR in PBS buffer at a concentration of $2.3 \times 10^5$ pfu $mL^{-1}$ using a peristaltic pump at a flow rate of 60 μL $min^{-1}$. The sensorgram showed that most of M13 binding occurred during the first 5 min. Eventually it took about 16 min for the bacteriophage to reach the saturation level. To confirm the bacteriophage immobilization, a secondary antibody with the same concentration was introduced into the OFRR. A clear red shift is indicative of the binding of the secondary antibody to the captured M13 virus on the capillary surface.

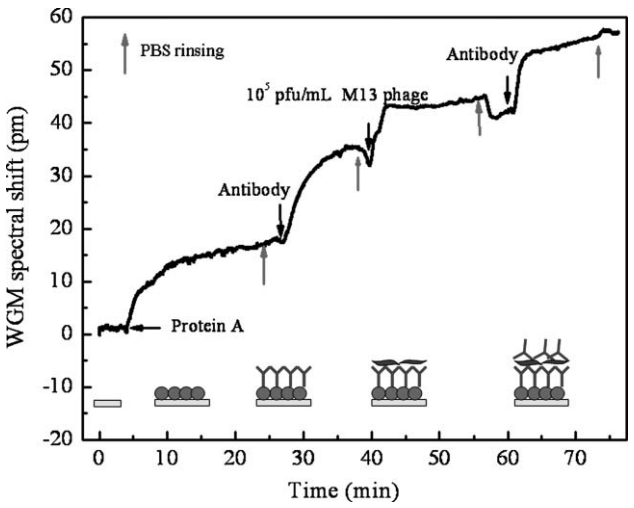


**Fig. 4** Sensorgram for immobilization of protein A and anti-M13 antibody to the sensing surface, and subsequent binding of the M13 filamentous phage and of the secondary antibody.

To further explore the detection limit and dynamic range of the OFRR for virus detection, bacteriophage solutions were passed through the sensing surface with increasing concentrations from $2.3 \times 10^3$ to $2.3 \times 10^{11}$ pfu $mL^{-1}$. Fig. 5 shows that the WGM spectral shift was gradually increased when the virus

 

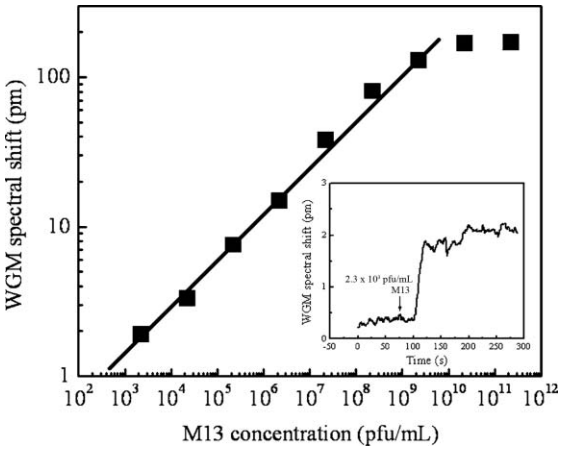


**Fig. 5** WGM spectral shift measured for various concentrations of M13 phage in PBS buffer. Concentration varied from $2.3 \times 10^3$ to $2.3 \times 10^{11}$ pfu mL$^{-1}$. Inset: WGM spectral shift for $2.3 \times 10^3$ pfu mL$^{-1}$ M13.

concentration increased from $2.3 \times 10^3$ to $2.3 \times 10^{10}$ pfu mL$^{-1}$ and reached the saturation level after $2.3 \times 10^{10}$ pfu mL$^{-1}$. The WGM spectral shift demonstrates that the OFRR has a dynamic range of seven orders of magnitude. As shown in the inset of Fig. 5, the experimental detection limit was $2.3 \times 10^3$ pfu mL$^{-1}$, which yielded an approximate 2 pm WGM shift, well above the system noise level. Note that this detection limit was achieved with the direct detection assay and without using secondary antibodies.

### Specificity of the OFRR for virus detection

Usually the biorecognition layers provide the specificity to the sensor. Herein, two assays were carried out to demonstrate the specificity of the OFRR for virus detection. First, the specificity of the anti-M13 antibody was tested. The sensing surface was modified with antibody following the same surface chemistry procedures. Instead of M13 phage, T4 phage with a concentration of $10^7$ pfu mL$^{-1}$ was then introduced into the OFRR as a negative control analyte. As shown in Fig. 6(A), there was virtually no WGM spectral shift observed after T4 phage injection, despite the very high concentration of T4. This clearly shows that the OFRR with antibody as a probe has very good specificity for the M13. In the second assay, protein A was immobilized on the sensing surface. As expected, when M13 phage with high concentration was introduced into the OFRR, no WGM shift was observed, as shown in Fig. 6(B). These two control experiments strongly suggest that the shift for the M13 in Fig. 4 was indeed caused by the specific binding between M13 and anti-M13 antibody, instead of non-specific adsorption of the M13 onto the OFRR surface.

### Theoretical analysis

We have established a linear relationship between the WGM shift and the molecule density on the OFRR surface, which provides the detailed quantitative analysis for the detection of molecules using OFRR:[21]

$$\frac{\delta\lambda}{\lambda} = \sigma_p \alpha_{ex} \frac{2\pi\sqrt{n_2^2 - n_3^2}}{\varepsilon_0 \lambda^2} \frac{n_2}{n_3^2} S \qquad (2)$$

where $\delta\lambda$ is the WGM spectral shift due to the biomolecules captured on the surface, $\sigma_p$ is the molecular surface density giving the number of molecules per unit area, $\alpha_{ex}$ is the excess polarizability of the analyte, and $n_2$ and $n_3$ are the RI of the OFRR wall (1.45) and the aqueous medium in the capillary core (1.33). $\varepsilon_0$ is the vacuum permittivity, $S$ is the BRIS of the OFRR, and $\lambda$ is the wavelength of the WGM.

First, we use eqn (2) to estimate the surface coverage of the antibody. Assuming that the excess polarizability is proportional to the molecular weight, anti-M13 antibody has a molecular weight of about 155 kDa, so its excess polarizability is estimated to be $(4\pi\varepsilon_0)$ $9.04 \times 10^{-21}$ cm$^3$.[25–26] Further assumption that each antibody occupies an area of 25 nm$^2$ on the surface leads to a total WGM shift of 300 pm when the surface is fully covered by antibody. Typically, the first layer antibody resulted in a WGM shift of 20 pm, as shown in Fig. 4, suggesting that 6.7% of the surface was covered by the antibody.

The density of M13 filamentous phage can also be estimated in a similar manner. M13 is about 900 nm in length and 10 nm in diameter. If the sensing surface is fully covered by M13 phage,

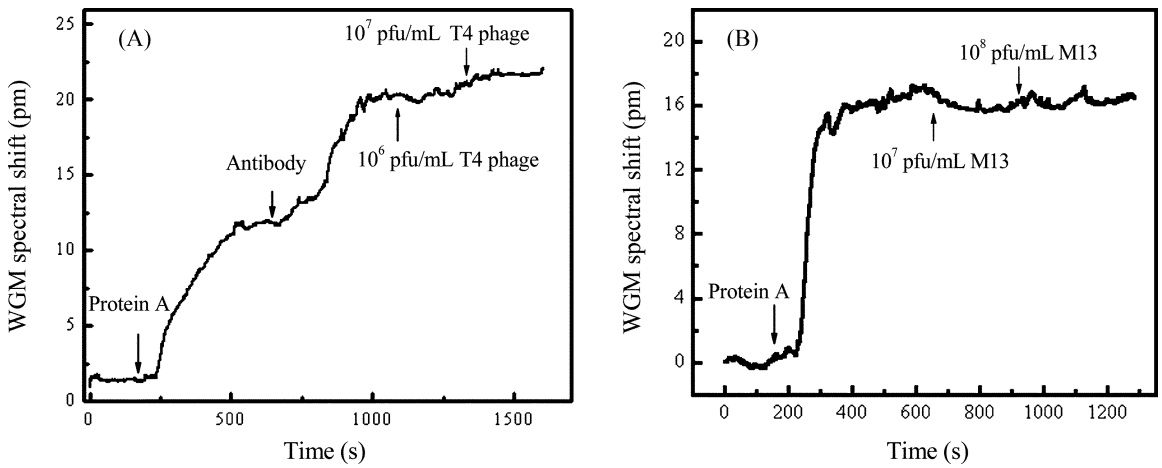


**Fig. 6** Control experiments for specificity test. (A) Sensorgram for immobilization of protein A, anti-M13 antibody, and subsequent binding of T4 phage. (B) Sensorgram for immobilization of protein A and subsequent binding of M13 phage.

the surface density is about $10^{10}$ cm$^{-2}$. The excess polarizability for M13 phage is calculated according to the method provided in ref. 27:

$$\alpha^{av} = 0.5(\alpha_l + \alpha_t) \quad (3)$$

where $\alpha_l$ and $\alpha_t$ are the longitudinal and transverse polarizability of the rod-like molecule, $\alpha^{av}$ is the average excess polarizability of the molecule randomly lying on the surface; and $\alpha^{av} = 4\pi\varepsilon_0$ ($5.1 \times 10^{-18}$ cm$^3$) based on eqn (3) with the phage's RI of 1.57.[28] According to eqn (2), we predict that the total amount of the WGM shift is 427 pm at the BRIS of 22 nm RIU$^{-1}$ when the surface is fully covered by M13. As shown in Fig. 4, $2.3 \times 10^5$ pfu mL$^{-1}$ caused a WGM shift of approximately 10 pm, which corresponds to 2.3% surface coverage. For the whole detection range ($2.3 \times 10^3$ to $2.3 \times 10^{10}$ pfu mL$^{-1}$), the WGM shift was 2–170 pm, corresponding to 0.5–40% surface coverage.

The theoretical detection limit can be estimated based on the experimental results. The detect limit is mainly limited by the $Q$-factor and temperature fluctuations. For $Q \approx 10^6$, which can be obtained with the OFRR, the WGM noise caused by temperature fluctuation becomes a dominant factor. With a thermo-electric cooler, the WGM noise (3 standard deviations) on the order of 0.02 pm has been achieved.[23] Therefore, for the OFRR with a BRIS of 22 nm RIU$^{-1}$, theoretically we can detect a concentration down to tens of viruses per mL and the surface density of only $5 \times 10^5$ cm$^{-2}$. Given the small OFRR size, this means there may be only a few viruses in the capillary detection region.

## Conclusion

In this study, we have developed a rapid and sensitive optical sensor for on-line virus detection based on the OFRR. The experimental detection limit was as low as $2.3 \times 10^3$ pfu mL$^{-1}$, with a dynamic range of seven orders of magnitude. The specificity of the sensor was tested by control experiments and the experimental results are verified with theoretical analysis. In the future, we will work on the real clinical samples and use the OFRR capillaries as vesicles for PCR reactions to provide more information about the analytes' entities. Furthermore, microfabricated waveguides will be employed in replacement of the fiber taper to realize the microarray chip for detecting and analyzing multiple viruses in a parallel manner. Finally, single virus detection will also be very interesting to pursue.

## Acknowledgements

The authors thank the very helpful discussion and the samples from Professor George Smith at the Division of Biological Science, the University of Missouri-Columbia. The financial support from the 3M Non-Tenured Faculty Award, the Wallace H. Coulter Early Career Award, and the Petroleum Research Fund (43879-G10) is acknowledged.

## References

1 R. Jenison, M. Rihanek and B. Polisky, *Biosens. Bioelectron.*, 2001, **16**, 757–763.
2 F. Komurian-Pradel, M. Perret, B. Deiman, M. Sodoyer, V. Lotteau, G. Paranhos-Baccalà and P. André, *J. Virol. Methods*, 2004, **116**, 103–106.
3 V. A. Olson, T. Laue, M. T. Laker, I. V. Babkin, C. Drosten, S. N. Shchelkunov, M. Niedrig, I. K. Damon and H. Meyer, *J. Clin. Microbiol.*, 2004, **42**, 1940–1946.
4 C. Steiniger, M. Kundi, S. W. Aberle, J. H. Aberle and T. Popow-Kraupp, *J. Clin. Microbiol.*, 2002, **40**, 2051–2056.
5 S. C. Zoth and O. Taboga, *J. Virol. Methods*, 2006, **138**, 99–108.
6 V. Kumarasamy, A. H. Wahab, S. K. Chua, Z. Hassan, Y. K. Chem, M. Mohamad and K. B. Chua, *J. Virol. Methods*, 2007, **140**, 75–79.
7 V. Guillaume, A. Lefeuvre, C. Faure, P. Marianneau, R. Buckland, S. K. Lam, T. F. Wild and V. Deubel, *J. Virol. Methods*, 2004, **120**, 229–237.
8 E. Uttenthaler, M. Schraml, J. Mandel and S. Drost, *Biosens. Bioelectron.*, 2001, **16**, 735–743.
9 E. Uttenthaler, C. KoÈûlinger and S. Drost, *Anal. Chim. Acta*, 1998, **362**, 91–100.
10 J. S. Yu, H. X. Liao, A. E. Gerdon, B. Huffman, R. M. Scearce, M. McAdams, S. M. Alam, P. M. Popernack, N. J. Sullivan, D. Wright, D. E. Cliffel, G. J. Nabel and B. F. Haynes, *J. Virol. Methods*, 2006, **137**, 219–228.
11 Y. G. Lee and K. S. Chang, *Talanta*, 2005, **65**, 1335–1342.
12 O. Tamarin, S. Comeau, C. Dejous, D. Moynet, D. Rebiere, J. Bezian and J. Pistre, *Biosens. Bioelectron.*, 2003, **18**, 755–763.
13 P. M. Boltovets, V. R. Boyko, I. Y. Kostikov, N. S. Dyachenko, B. A. Snopok and Y. M. Shirshov, *J. Virol. Methods*, 2002, **105**, 141–146.
14 P. M. Boltovets, B. A. Snopok, V. R. Boyko, T. P. Shevchenko, N. S. Dyachenko and Y. M. Shirshov, *J. Virol. Methods*, 2004, **121**, 101–106.
15 J. W. Chung, S. D. Kim, R. Bernhardt and J. C. Pyun, *Sens. Actuators, B*, 2005, **111**, 416–422.
16 K. A. Donaldson, M. F. Kramer and D. V. Lim, *Biosens. Bioelectron.*, 2004, **20**, 322–327.
17 B. H. Schneider, J. G. Edwards and N. F. Hartman, *Clin. Chem. (Washington, D. C.)*, 1997, **43**, 1757–1763.
18 A. Ymeti, J. Greve, P. V. Lambeck, T. Wink, S. W. F. M. V. Hövell, T. A. M. Beumer, R. R. Wijin, R. G. Heideman, V. Subramaniam and J. S. Kanger, *Nano Lett.*, 2007, **7**, 394–397.
19 S. Arnold, R. Ramjit, D. Keng, V. Kolchenko and I. Teraoka, *Faraday Discuss.*, 2008, **137**, 65–83.
20 I. M. White, H. Oveys and X. Fan, *Opt. Lett.*, 2006, **31**, 1319–1321.
21 H. Zhu, I. M. White, J. D. Suter, P. S. Dale and X. Fan, *Opt. Express*, 2007, **15**, 9139–9146.
22 J. D. Suter, I. M. White, H. Zhu, D. H. Shi, C. W. Caldwell and X. Fan, *Biosens. Bioelectron.*, DOI: 10.1016/j.bios.2007.10.005.
23 H. Zhu, I. M. White, J. D. Suter, M. Zourob and X. Fan, *Anal. Chem.*, 2007, **79**, 930–937.
24 S. I. Shopova, H. Zhu, X. Fan and P. Zhang, *Appl. Phys. Lett.*, 2007, **90**, 221101.
25 F. Vollmer, D. Braun, A. Libchaber, M. Khoshsima, I. Teraoka and S. Arnold, *Appl. Phys. Lett.*, 2002, **80**, 4057–4059.
26 S. Arnold, M. Khoshsima, I. Teraoka, S. Holler and F. Vollmer, *Opt. Lett.*, 2003, **28**, 272–274.
27 Z. Salamon and G. Tollin, *Biophys. J.*, 2001, **80**, 1557–1567.
28 V. Nanduri, S. Balasubramanian, S. Sista, V. J. Vodyanoy and A. L. Simonian, *Anal. Chim. Acta*, 2007, **589**, 166–172.

 